Identification of Solar Collector Dynamics Using Physical Model-Based Approach

B. J. Huang
Professor.

S. B. Wang
Graduate Assistant.

Department of Mechanical Engineering,
National Taiwan University,
Taipei, Taiwan 10764

A system dynamics model of flat-plate solar collectors was derived and identified here. A nonlinear physical model was first derived from a two-node concept and energy conservation principle. The model was then approximated by the linear perturbation equations which were Laplace transformed and solved to lead to a distributed model in terms of the transfer functions. A model reduction was further employed to yield a linear time-invariant model with parameters as functions of steady-state operating conditions. The model parameters were identified by a dynamic test with step inputs at various operating conditions using frequency response analysis and model fitting in frequency domain. The identified parameters were then fitted to a function of steady-state mass flowrate $\overline{m}_w$. Thus, the model can describe the system dynamics behavior under various operating conditions through the identified parameters. The simulations using the model were shown to agree very well with the test results.

I Introduction

The understanding of system dynamics behavior of solar collectors is quite important in the controller design of solar hot water systems, the transient performance analysis of solar thermosyphon systems, and the development of collector efficiency test methods. One-node capacitance model of flat-plate collectors has been closely derived [1] which assumes that the structural material of the collector and the fluid flowing inside the collector can be lumped together with a single uniform temperature (i.e., one node). A two-node capacitance model was further derived by Klein et al. [2] by separately lumping the flat plate and the glass cover as two nodes with two individual uniform temperatures. The flat plate was additionally assumed to be lumped together with the fluid at the mean fluid temperature. The solar collector is essentially a heat exchanger and its dynamic behavior is nonlinear. However, the dynamic model can become a distributed model if linearization has been applied.

De Ron [3] considered the temperature variations of glass cover, flat plate, and fluid in the flow direction. A distributed model of a flat-plate collector was theoretically derived by use of linear perturbation. An indoor experiment was performed to measure the frequency responses of the collector using binary multifrequency test signals for verifying the theoretical model. The system dynamics model of the collector will hopefully be a standard transfer-function form for practical applications. However, the model parameters in De Ron's model [3] are all presented in terms of the heat capacitances, optical properties of black surface, heat transfer coefficients, fluid properties, etc. which can only be theoretically evaluated and thus could cause a large error.

The system dynamics model of solar collectors can also be identified by least-squares estimation method associated with a structure such as ARMAX, ARX, Box-Jenkins models etc. However, the parameters identified in this way provides only numerical values and would vary with operating conditions. It is very difficult to correlate the model parameters with the operating conditions without the guideline of a physical model. The parameter variation with operating conditions in a linear system is usually caused by the nonlinear effects and should be determined accurately in order to design a better controller. An attempt has been made here to overcome this problem to derive a linear dynamic model of solar collector with parameters varying with the steady-state operating conditions by using a so-called *physical model-based approach*.

II Derivation of Dynamic Model

2.1 Basic Assumptions and Governing Equations. For flat-plate collectors, the absorbed solar energy is trans-

Contributed by the Dynamic Systems and Control Division for publication in the JOURNAL OF DYNAMIC SYSTEMS, MEASUREMENT, AND CONTROL. Manuscript received by the DSCD September 12, 1989. Associate Technical Editor: P. Usoro.

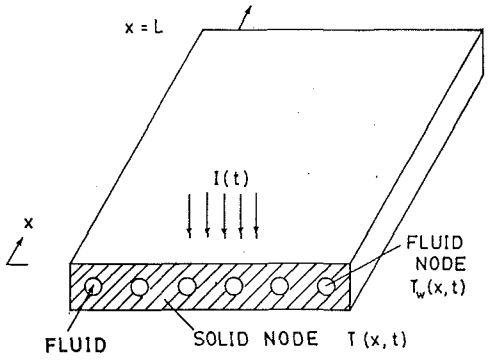

Fig. 1 Schematic diagram of a 2-node collector model

ferred from the flat plate to the working fluid as the useful energy and to the ambient as the heat loss. The flat-plate collector can be divided into solid and fluid phases or nodes i.e., two nodes in order to facilitate the analysis (Fig. 1). The solid node consists of glass cover, flat plate, insulating material, and structural materials etc.; the fluid node is, meanwhile, only the working fluid flowing through the collector. All the constructing materials of the solid node are assumed to be lumped together with a temperature T_s. However, the temperature variation of the solid node along x is considered in order to account for the variation of heat transfer along the flow direction. The solid node temperature is then a function of position and time, i.e., $T_s(x, t)$.

The conduction heat transfer within the solid node is relatively small as compared to the convective heat transfer occurred adjacent to the fluid-wall boundary. This is since the Biot number is usually small for flat-plate collectors. Additionally, constant physical properties for the fluid and the solid nodes and a uniform flow distribution is assumed here to exist in the collector and the effect of wind speed variation on the heat loss is neglected. An energy balance has made to the solid node then yields:

$$M_s C_s \frac{\partial T_s(x,t)}{\partial t} = I(t)(\tau\alpha)_e A_b - h_w A_w [T_s(x,t) - T_w(x,t)] - h_a A_b [T_s(x,t) - T_a(t)]. \quad (1)$$

Energy balance to the fluid node yields

$$M_w C_w \frac{\partial T_w(x,t)}{\partial t} = h_w A_w [T_s(x,t) - T_w(x,t)] - m_w(t) C_w L \frac{\partial T_w(x,t)}{\partial x}, \quad (2)$$

where T_s and T_w are, respectively, the solid-node and the fluid-node temperatures; $I(t)$ is the solar irradiation incident upon the collector slope; $(\tau\alpha)_e$ is the effective transmittance-absorptance of collector; M_s and M_w are, respectively, the masses of the solid and fluid nodes; C_s and C_w are, respectively, the heat capacities of the solid and fluid nodes; h_a is the heat transfer coefficient defined from the solid node to

Nomenclature

A_b = black surface area, m^2
A_w = total area between fluid and plate in the collector, m^2
C_s = heat capacity of plate, J/kg°C
C_w = heat capacity of water, J/kg°C
f = frequency, Hz
$G(s)$ = transfer function of the plant model
h_a = convective heat transfer coefficient of air, W/m^2°C
h_w = convective coefficient between the fluid and the solid nodes, W/m^2°C
$\bar{h}_w$ = convective coefficient between the fluid and the solid nodes at steady state, W/m^2°C
I = irradiation upon the collector slope, W/m^2
k_I = system gain of the disturbance model $W(s)$, °Cm^2/W
k_w = system gain of the disturbance model $G(s)$, °Cs/kg
L = collector length, m
M = mass of solid or fluid node, kg
m_w = mass flowrate, kg/s
p_{I1} = pole of the disturbance model $W(s)$, s^{-1}
p_{I2} = pole of the disturbance model $W(s)$, s^{-1}
p_{w1} = pole of the disturbance model $G(s)$, s^{-1}
p_{w2} = pole of the disturbance model $G(s)$, s^{-1}
s = Laplace transform variable
T_a = ambient temperature, °C
T_e = $T_w(L, t)$ = collector exit temperature, °C
T_i = $T_w(0, t)$ = collector inlet temperature, °C
T_s = solid-node temperature, °C
T_w = fluid-node or water temperature, °C
ΔT_{ei} = $T_e - T_i$, °C
t = time, s
$u(t)$ = unit step function, dimensionless
$W(s)$ = transfer function of the disturbance model
x = coordinate along the flow direction, m
y = direct output signal of the plant model $G(s)$, °C
z = the measured output signal, °C
z_w = zero of the disturbance model $G(s)$, s^{-1}
β = Eq. (10)
$\delta(t)$ = delta function
ω = frequency, rad/s
τ_w = time constant of the fluid phase, eqn (10)
τ_{pa} = time constant of the plate due to air convection, eqn (10)
τ_{pw} = time constant of the plate due to water convection, eqn (10)
$(\tau\alpha)_e$ = absorption of black surface
γ = Eq. (10)

Subscript

a = ambient; air
w = water; fluid phase
s = solid phase; plate
i = collector inlet
e = collector exit

Superscript

$\bar{}$ = steady-state value; mean value
$\tilde{}$ = perturbation

the ambient air; h_w is the convective heat transfer coefficient from the solid node to the fluid node; m_w is the mass flowrate through the collector; L is the collector length; A_b is the black surface area of the solid node; A_w is the total contact area between the fluid and solid nodes.

2.2 Linear Perturbation Model. The governing Eqs. (1) and (2) are nonlinear. This is essentially caused by the coupling of the mass flowrate $m_w(t)$ with the fluid-node temperature $T_w(x, t)$ in Eq. (2) and the variation of heat transfer coefficient h_w with the mass flowrate $m_w(t)$ which may in turn be coupled with $T_w(x, t)$, $T_s(x, t)$ and $T_a(t)$ as shown in Eqs. (1) and (2). A linearization around a steady-state point using the following perturbations is thus necessary:

$$T_s(x, t) = \bar{T}_s(x) + \tilde{T}_s(x, t) \tag{3}$$

$$T_w(x, t) = \bar{T}_w(x) + \tilde{T}_w(x, t) \tag{4}$$

$$T_a(t) = \bar{T}_a + \tilde{T}_a(t) \tag{5}$$

$$I(t) = \bar{I} + \tilde{I}(t) \tag{6}$$

$$m_w(t) = \bar{m}_w + \tilde{m}_w(t) \tag{7}$$

By substituting Eqs. (3)–(7) into Eqs. (1) and (2), and assuming constant h_a, one obtains

$$\frac{\partial \tilde{T}_s(x, t)}{\partial t} = \frac{\bar{I} + \tilde{I}(t)}{\gamma} - \frac{[\bar{T}_s(x) + \tilde{T}_s(x, t)] - [\bar{T}_w(x) + \tilde{T}_w(x, t)]}{\tau_{pw}} - \frac{[\bar{T}_s + \tilde{T}_s(x, t)] - [\bar{T}_a + \tilde{T}_a(t)]}{\tau_{pa}} \tag{8}$$

$$\frac{\partial \tilde{T}_s(x, t)}{\partial t} = \frac{[\bar{T}_s(x) + \tilde{T}_s(x, t)] - [\bar{T}_w(x) + \tilde{T}_w(x, t)]}{\tau_w} - [\bar{m}_w + \tilde{m}_w(t)]\beta \frac{\partial[\bar{T}_w(x) + \tilde{T}_w(x, t)]}{\partial x} \tag{9}$$

where

$$\tau_{pw} \equiv \frac{M_s C_s}{\bar{h}_w A_w};\ \tau_{pa} \equiv \frac{M_s C_s}{h_a A_b};\ \gamma \equiv \frac{M_s C_s}{(\tau\alpha)_e A_b};\ \tau_w \equiv \frac{M_w C_w}{\bar{h}_w A_w};\ \beta \equiv \frac{C_w L}{M_w C_w}, \tag{10}$$

where $\bar{h}_w$ is the heat transfer coefficient at steady-state operating condition.

Equations (8) and (9) at steady states turn out to be

$$0 = \frac{\bar{I}}{\gamma} - \frac{\bar{T}_s - \bar{T}_w}{\tau_{pw}} - \frac{\bar{T}_s - \bar{T}_a}{\tau_{pa}} \tag{11}$$

$$0 = \frac{\bar{T}_s - \bar{T}_w}{\tau_w} - \bar{m}_w \beta \frac{d\bar{T}_w(x)}{dx}. \tag{12}$$

The steady-state solutions are obtained from Eqs. (11) and (12):

$$\bar{T}_s(x) = \frac{\tau_{pw}\tau_{pa}}{\tau_{pw} + \tau_{pa}}\left[\frac{\bar{I}}{\gamma} + \frac{\bar{T}_w(x)}{\tau_{pw}} + \frac{\bar{T}_a}{\tau_{pa}}\right] \tag{13}$$

$$\bar{T}_w(x) = \tau_{pa}\left(\frac{\bar{I}}{\gamma} + \frac{\bar{T}_a}{\tau_{pa}}\right) + \left[\bar{T}_i - \tau_{pa}\left(\frac{\bar{I}}{\gamma} + \frac{\bar{T}_a}{\tau_{pa}}\right)\right] \exp\left\{\frac{-\tau_{pw}x}{\tau_w \bar{m}_w \beta (\tau_{pw} + \tau_{pa})}\right\}, \tag{14}$$

By substituting the steady-state solutions into Eqs. (8) and (9), one obtains

$$\frac{\partial \tilde{T}_s(x, t)}{\partial t} = \frac{\tilde{I}(t)}{\gamma} - \frac{\tilde{T}_s(x, t) - \tilde{T}_w(x, t)}{\tau_{pw}} - \frac{\tilde{T}_s(x, t) - \tilde{T}_a(t)}{\tau_{pa}} \tag{15}$$

$$\frac{\partial \tilde{T}_w(x, t)}{\partial t} = \frac{\tilde{T}_s(x, t) - \tilde{T}_w(x, t)}{\tau_w} - \bar{m}_w \beta \frac{\partial \tilde{T}_w(x, t)}{\partial x} - \frac{\tilde{m}_w(t)}{\tau_w \bar{m}_w}\left[\frac{\tau_{pw}\tau_{pa}}{\tau_{pw} + \tau_{pa}}\left(\frac{\bar{I}}{\gamma} - \frac{\bar{T}_w(x)}{\tau_{pa}} + \frac{\bar{T}_a}{\tau_{pa}}\right)\right]. \tag{16}$$

Equations (15) and (16) represent the linear perturbation model of the flat-plate collector around a steady-state operating condition.

2.3 System Transfer-Function Model. To derive a system transfer-function model, Laplace transform of Eqs. (15) and (16) is first taken here with respect to time t and $\tilde{T}_s(x, s)$ is eliminated to obtain

$$\frac{d\tilde{T}_w(x, s)}{dx} + D(s)\tilde{T}_w(x, s) = E(s) + F(s)e^{-Ax} \tag{17}$$

where $D(s)$, $E(s)$ and $F(s)$ are defined as

$$D(s) \equiv \frac{1}{\bar{m}_w \beta}\left[\frac{\tau_{pa}\tau_{pw}\tau_w s^2 + (\tau_{pa}\tau_{pw} + \tau_{pa}\tau_w + \tau_{pw}\tau_w)s + \tau_{pw}}{\tau_{pa}\tau_{pw}\tau_w s + \tau_{pa}\tau_w + \tau_{pw}\tau_w}\right] \tag{18}$$

$$E(s) \equiv \left\{\frac{\tilde{I}(s)}{\gamma\tau_w\left(s + \frac{1}{\tau_{pw}} + \frac{1}{\tau_{pa}}\right)} + \frac{\tilde{T}_a(s)}{\tau_{pa}\tau_w\left(s + \frac{1}{\tau_{pw}} + \frac{1}{\tau_{pa}}\right)}\right\}\frac{1}{\bar{m}_w \beta} \tag{19}$$

$$F(s) \equiv \frac{\tilde{m}_w(s)\tau_{pw}\left[\bar{T}_i - \frac{B}{A}\right]}{\tau_w(\tau_{pw} + \tau_{pa})\bar{m}_w^2 \beta} \tag{20}$$

$$A \equiv \frac{\tau_{pw}}{\tau_w \bar{m}_w \beta (\tau_{pw} + \tau_{pa})};\quad B \equiv \frac{1}{\tau_w \bar{m}_w \beta}\left[\frac{\tau_{pw}\tau_{pa}}{\tau_{pw} + \tau_{pa}}\left(\frac{\bar{I}}{\gamma} + \frac{\bar{T}_a}{\tau_{pa}}\right)\right]. \tag{21}$$

By solving Eq. (17) for $\tilde{T}_w(x, s)$, one obtains

$$\tilde{T}_w(x, s) = H_{in}(x, s)\tilde{T}_i(s) + H_I(x, s)\tilde{I}(s) + H_a(x, s)\tilde{T}_a(s) + H_m(x, s)\tilde{m}_w(s) \tag{22}$$

where

$$H_{in}(x, s) = e^{-D(s)x} \tag{23}$$

$$H_I(x, s) = \frac{1 - e^{-D(s)x}}{\tau_{pa}\tau_{pw}\tau_w s^2 + (\tau_{pa}\tau_w + \tau_{pw}\tau_w + \tau_{pa}\tau_{pw})s + \tau_{pw}} \frac{\tau_{pa}\tau_{pw}}{\gamma} \tag{24}$$

$$H_a(x, s) = \frac{[1 - e^{-D(s)x}]\tau_{pw}}{\tau_{pa}\tau_{pw}\tau_w s^2 + (\tau_{pa}\tau_w + \tau_{pw}\tau_w + \tau_{pa}\tau_{pw})s + \tau_{pw}} \tag{25}$$

$$H_m(x, s) = \frac{\tau_{pw}\left[\overline{T}_i - \frac{B}{A}\right]\left[e^{-Ax} - e^{-D(s)x}\right]}{\beta \overline{m}_w^2 \tau_w (\tau_{pa} + \tau_{pw})\,[D(s) - A]},$$

where $\overline{T}_i$ is the inlet temperature at steady state, i.e., $\overline{T}_w(0)$; $\tilde{T}_i(s) \equiv \tilde{T}_w(0, s)$.

Equations (22)–(26) represent the system transfer-function model of a flat-plate collector which is a distributed system. The response of collector outlet temperature $\tilde{T}_e(s) \equiv \tilde{T}_w(L, s)$ is of our practical major interest. Thus, by letting $x = L$, one obtains

$$\tilde{T}_e(s) = H_{in}(L, s)\tilde{T}_i(s) + H_I(L, s)\tilde{I}(s) + H_a(L, s)\tilde{T}_a(s) + H_m(L, s)\tilde{m}_w(s) \tag{27}$$

where

$$H_{in}(L, s) = e^{-D(s)L} \tag{28}$$

$$W(s) \equiv H_I(L, s) = \frac{1 - e^{-D(s)L}}{\tau_{pa}\tau_{pw}\tau_w s^2 + (\tau_{pa}\tau_w + \tau_{pw}\tau_w + \tau_{pa}\tau_{pw})s + \tau_{pw}} \frac{\tau_{pa}\tau_{pw}}{\gamma} \tag{29}$$

$$H_a(L, s) = \frac{[1 - e^{-D(s)L}]\tau_{pw}}{\tau_{pa}\tau_{pw}\tau_w s^2 + (\tau_{pa}\tau_w + \tau_{pw}\tau_w + \tau_{pa}\tau_{pw})s + \tau_{pw}} \tag{30}$$

$$G(s) \equiv H_m(L, s) = \frac{\tau_{pw}\left[\overline{T}_i - \frac{B}{A}\right]\left[e^{-AL} - e^{-D(s)L}\right]}{\beta \overline{m}_w^2 \tau_w (\tau_{pa} + \tau_{pw})\,[D(s) - A]}. \tag{31}$$

The outlet temperature responses $\tilde{T}_e$ can be seen from Eqs. (28)–(31) to consist of an exponential term $e^{-D(s)L}$ which implies the presence of a high-order effect. The flat-plate solar collector usually behaves low-pass property in practical designs even though the system dynamics behavior due to the high-order term $e^{-D(s)L}$ may involve multiple poles and zeros. An order reduction is then possible since the high-order effect is only significant at a high frequency which is usually outside the range of practical applications.

2.4 Model Reduction. The system transfer functions represented by Eqs. (28) through (30) can interestingly enough be exactly obtained if the above derivation is repeated by assuming a linear fluid temperature distribution at steady states, i.e., $\frac{\overline{T}_w(x)}{dx} = r$ = constant, which usually holds for flat-plate collectors (Fig. 2). The design parameters of the solar collector used to generate Figure 2 are: $\overline{I} = 1000$ W/m^2, $\overline{m}_w = 0.05$ kg/s, $\tau_{pw} = 92$ s, $\tau_{pa} = 726$ s, $\tau_w = 40$ s, $\gamma = 9597$ J/m^2°C, $\beta = 1.06$ m/kg, which is a general design of flat-plate collectors.

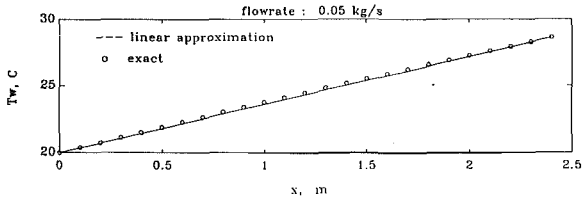

Fig. 2 Fluid temperature distributions inside the collector

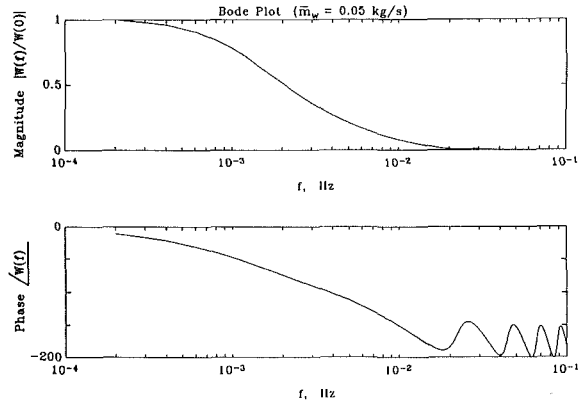

Fig. 3 Higher-order effect of $W(s)$

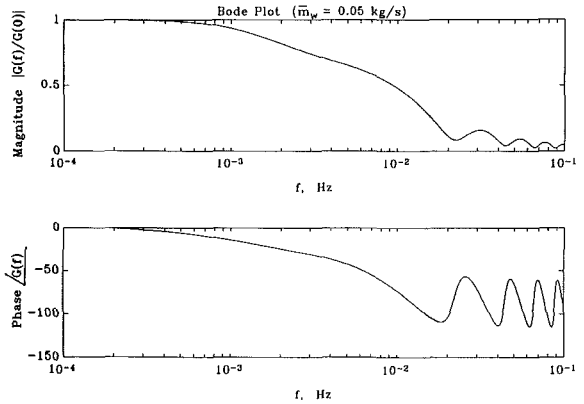

Fig. 4 Higher-order effect of $G(s)$

As to the transfer function $G(s)$, it then becomes

$$G(s) \equiv H_m(L, s) = \frac{\beta\gamma}{\tau_w \overline{m}_w} \left[1 - e^{-D(s)L}\right]\left[\frac{\tau_{pw}\tau_{pa}}{\tau_{pw} + \tau_{pa}}\left(\frac{\overline{I}}{\gamma} - \frac{\overline{T}_w}{\tau_{pa}} + \frac{\overline{T}_a}{\tau_{pa}}\right)\right] \times \frac{(\tau_{pa}\tau_{pw}\tau_w s + \tau_{pa}\tau_{pw} + \tau_{pa}\tau_w + \tau_{pw}\tau_w)}{\tau_{pa}\tau_{pw}\tau_w s^2 + (\tau_{pa}\tau_{pw} + \tau_{pa}\tau_w + \tau_{pw}\tau_w)s + \tau_{pw}} \tag{32}$$

The system model can then be represented by Eqs. (27)–(30), and (32), which still consist of a high-order term $e^{-D(s)L}$. Further order reduction is possible if the frequency response or Bode plots are examined here (Figs. 3 and 4). The design parameters of the solar collector used to generate Figs. 3 and 4 are the same as those used in Fig. 2.

The system dynamics model $W(s)$ can be seen from Eq. (29) to be second order (i.e., containing a second-order polynomial or two poles in the denominator) with a high-order

term $1 - e^{-D(s)L}$ in the numerator. The phase plot of $W(\omega)$ is revealed by Fig. 3 to approach −180 deg at frequency > 0.02 Hz which is a second-order behavior if the oscillation has been ignored. This indicates that the oscillation of the phase plot shown in Figure 3 has mainly resulted from the high-order term $1 - e^{-D(s)L}$.

$W(s)$ can be further modified by replacing the high-order term $1 - e^{-D(s)L}$ with a time delay term $e^{-\tau_{dI}s}$. This is since the gain of $W(\omega)$ drops −20 db at frequency > 0.01 Hz and the flat-plate solar collector usually operates at frequency < 0.01 Hz in field applications due to relatively slow variation of solar irradiation.

The system dynamics model $G(s)$ is similarly shown by Eq. (32) to be also of second order (i.e., containing a second-order polynomial or two poles in the denominator) with a zero (containing a first-order polynomial in the denominator) and a high-order term $1 - e^{-D(s)L}$ in the numerator. The phase plot of $G(\omega)$ approaches −90 deg with oscillation at frequency > 0.02 Hz as revealed in Fig. 4. This implies that the number of zeros will be less than the number of poles by one if the oscillation was ignored. This coincides with the dynamic model of equation (32) if the high-order term $1 - e^{-D(s)L}$ was ignored. The above evidences indicate that the oscillation of the phase plot shown in Fig. 4 mainly resulted from the high-order term $1 - e^{-D(s)L}$.

The gain of $G(\omega)$ drops −20 db at frequency > 0.02 Hz as shown in Fig. 4. However, the flat-plate solar collector usually operates at frequency < 0.01 Hz due to a slow variation of mass flowrate in field applications. Hence, $G(s)$ can be further modified by replacing the high-order term $1 - e^{-D(s)L}$ with a time delay term $e^{-\tau_{dw}s}$.

The oscillations of the gain and phase plots of $W(s)$ and $G(s)$ as shown in Figs. 3 and 4 are very typical in some distributed systems such as heat exchanger dynamics [4–6]. The frequency response of $W(s)$ and $G(s)$ shown in Figs. 3 and 4 depicts that the higher order effect is significantly revealed only at a high frequency. The system transfer functions as a result of the above model reduction procedures finally become

$$H_{in}(L, s) = e^{-D(s)L} \tag{28}$$

$$H_a(L, s) = \frac{e^{-\tau_{da}s}\tau_{pw}}{\tau_{pa}\tau_{pw}\tau_w s^2 + (\tau_{pa}\tau_w + \tau_{pw}\tau_w + \tau_{pa}\tau_{pw})s + \tau_{pw}} \tag{33}$$

$$W(s) = \frac{e^{-\tau_{dI}s}}{\tau_{pa}\tau_{pw}\tau_w s^2 + (\tau_{pa}\tau_w + \tau_{pw}\tau_w + \tau_{pa}\tau_{pw})s + \tau_{pw}} \frac{\tau_{pa}\tau_{pw}}{\gamma} \tag{34}$$

$$G(s) = \frac{\beta\gamma}{\tau_w \bar{m}_w} \frac{e^{-\tau_{dw}s}\left[\frac{\tau_{pw}\tau_{pa}}{\tau_{pw}+\tau_{pa}}\left(\frac{\bar{I}}{\gamma} - \frac{\bar{T}_w}{\tau_{pa}} + \frac{\bar{T}_a}{\tau_{pa}}\right)\right] \times (\tau_{pa}\tau_{pw}\tau_w s + \tau_{pa}\tau_{pw} + \tau_{pa}\tau_w + \tau_{pw}\tau_w)}{\tau_{pa}\tau_{pw}\tau_w s^2 + (\tau_{pa}\tau_{pw} + \tau_{pa}\tau_w + \tau_{pw}\tau_w)s + \tau_{pw}} \tag{35}$$

In most of solar systems, the collector inlet fluid temperature T_i and the ambient temperature T_a usually vary very slowly. The identification of transfer functions $H_{in}(L, s)$ and $H_a(L, s)$ are then not important in the differential-temperature (DT) controller design or other applications. Therefore, only $W(s)$ and $G(s)$ were identified in the present study and the system block diagram becomes Fig. 5. The mass flowrate $\tilde{m}_w$ is a controllable input variable in practice and the incident irradiation $\tilde{I}$ acts as an uncontrollable input to solar collector. Thus, $G(s)$ can be considered as the plant model; $W(s)$ is meanwhile considered the disturbance model.

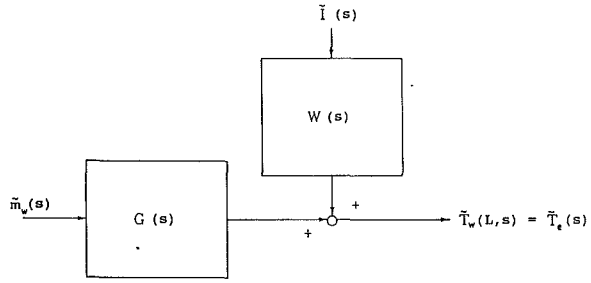

Fig. 5 Simplified system block diagram

The model structure represented by Eqs. (34) and (35) can be further expressed in the form

$$W(s) \equiv \frac{\tilde{T}_e(s)}{\tilde{I}(s)} = \frac{e^{-\tau_{dI}s}k_I}{\left(\frac{s}{p_{I1}} + 1\right)\left(\frac{s}{p_{I2}} + 1\right)} \tag{36}$$

$$G(s) \equiv \frac{\tilde{T}_e(s)}{\tilde{m}_w(s)} = \frac{e^{-\tau_{dw}s}k_w(s/z_w + 1)}{\left(\frac{s}{p_{w1}} + 1\right)\left(\frac{s}{p_{w2}} + 1\right)} \tag{37}$$

where k_I and k_w are the system gains; p_{I1}, p_{I2}, p_{w1}, p_{w2} are the system poles; z_w is the system zero; all of these are functions of τ_{pa}, τ_{pw}, τ_w, γ, β as shown in the following equations:

$$k_I = \frac{\tau_{pa}}{\gamma};\ p_{I1}p_{I2} = \frac{1}{\tau_{pa}\tau_w};\ \frac{1}{p_{I1}} + \frac{1}{p_{I2}} = \frac{\tau_{pa}\tau_{pw} + \tau_{pa}\tau_w + \tau_{pw}\tau_w}{\tau_{pw}} \tag{38}$$

$$k_w = \frac{\beta\gamma}{\tau_w \bar{m}_w}\left[\frac{\tau_{pa}}{\tau_{pw}+\tau_{pa}}\left(\frac{\bar{I}}{\gamma} - \frac{\bar{T}_w}{\tau_{pa}} + \frac{\bar{T}_a}{\tau_{pa}}\right)\right] \Big/ (\tau_{pa}\tau_{pw} + \tau_{pa}\tau_w + \tau_{pw}\tau_w)\, z_w = \frac{\tau_{pa}\tau_{pw} + \tau_{pa}\tau_w + \tau_{pw}\tau_w}{\tau_{pa}\tau_{pw}\tau_w} \tag{39}$$

$$p_{w1}p_{w2} = \frac{1}{\tau_{pa}\tau_w};\ \frac{1}{p_{w1}} + \frac{1}{p_{w2}} = \frac{\tau_{pa}\tau_{pw} + \tau_{pa}\tau_w + \tau_{pw}\tau_w}{\tau_{pw}} \tag{40}$$

The poles of $W(s)$ and $G(s)$ are shown by the above relations to possibly be identical, i.e., $p_{w1} = p_{I1}$ and $p_{w2} = p_{I2}$. However, the distinct poles for $W(s)$ and $G(s)$, i.e., $p_{w1} \neq p_{I1}$ and $p_{w2} \neq p_{I2}$, are assumed here in order to account for the unmodelled dynamics due to the use of the 2-node concept, ignorance of wind speed effect, and assumptions of constant physical properties and uniform flow distribution, etc. The system parameters were estimated experimentally, since theoretical prediction of τ_{pa}, τ_{pw}, τ_w, γ, β and τ is not accurate.

Table 1 Design specification of flat-plate collector

Flat-plate design:	Tube-in-sheet
Flat-plate material:	Tube—copper (11mm diameter, 10 tubes)
	Sheet—extruded aluminum alloy (1mm thick)
Dimension:	231cm × 122cm
Black surface:	Nonselective paint
Black surface area:	$2.8m^2$
Glaze:	Single glass
Insulation:	25mm fiber glass

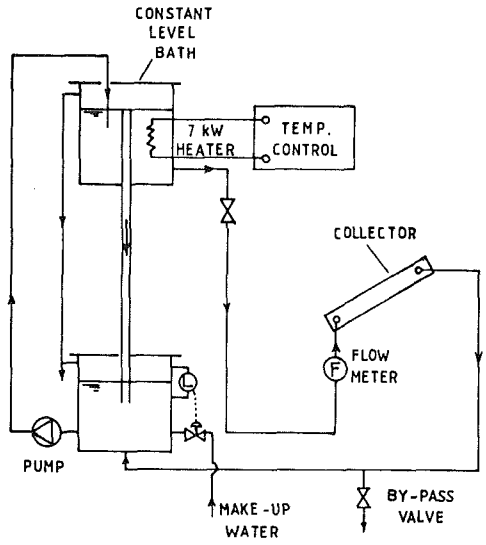

Fig. 6 Schematic diagram of the test system

III Parameter Estimation

3.1 Experimental Setup. An outdoor experiment was performed to identify the system parameters. The design specifications of the flat-plate solar collector used in the present experiment are listed in Table 1. The test system is shown in Fig. 6. A constant-level bath was used to supply a steady flow to the collector. An electric heater was installed within the upper bath and controlled by a digital controller to regulate the collector inlet temperature T_i to within ±0.5°C [7].

The data acquisition system consists of a PC, a YEW3880 hybrid recorder and a IEEE-488 interface. The sampling rate in the present experiment was 0.5 Hz. A SS-100 solar cell sensor was installed on the collector slope to measure the incident irradiation with an uncertainty of ±2 percent; a 3-cup windmeter was used to measure the wind speed with an uncertainty of ±0.2m/s; T-type thermocouples were used to measure the temperatures at the collector inlet and outlet, the constant-level bath, and the ambient with an uncertainty of ±0.1°C obtained by a calibration against a HP2804 precise quartz thermometer (with an uncertainty of ±0.04°C). A specially-designed thermopile was used to measure the temperature difference across the collector ΔT_{ei} with an uncertainty of ±0.07°C [8]. The mass flowrate was measured by a turbine flowmeter MK-508 with an uncertainty of ±20 cc/min.

3.2 Test Signal and Signal Processing

1 Input Test Signal. Step response tests were performed in the present study. To identify the disturbance model $W(s)$, a step of $\tilde{I}$ under a steady mass flowrate (i.e., letting $\tilde{m}_w = 0$) was applied and the temperature response ΔT_{ei} was measured. Negative step of $\tilde{I}$ was applied in the experiment by shading the collector at time $t = 0$ using a polylon board covered with aluminum foil. That is, the irradiation is suddenly reduced to zero to produce a negative step change of $\tilde{I}$. This step change is apparently not a small perturbation. It can actually be seen from the governing Eq. (1) that the collector dynamic response is linear in respect to the irradiation $I(s)$. This was also verified by many tests performed to determine the time constant of collectors [7]. The small perturbation in the linearization of I may therefore not be necessary and the use of a large negative step on $\tilde{I}$ in the dynamic test holds. The perturbed irradiation $\tilde{I}(t)$ can be mathematically written as

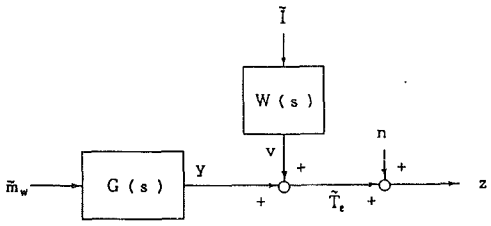

Fig. 7 Schematic diagram of the signal flow

$$\tilde{I}(t) = -\bar{I}u(t) \tag{41}$$

where $u(t)$ is the unit step function and $\bar{I}$ is the steady irradiation before the step change. The perturbed collector exit temperature $\tilde{T}_e(t)$ was evaluated by the following relation:

$$\tilde{T}_e(t) \equiv \tilde{T}_w(L, t) = \Delta T_{ei}(t) - \overline{\Delta T_{ei}} \tag{42}$$

where $\Delta T_{ei}(t) \equiv T_e(t) - T_i$; $\overline{\Delta T_{ei}} \equiv \bar{T}_e - T_i$, T_i is the inlet temperature which was maintained constant during the test.

A step of $\tilde{m}_w$ was produced under a steady irradiation i.e., $\tilde{I} = 0$ from a steady mass flowrate $\bar{m}_w$ in order to identify the model $G(s)$. The step change of $\tilde{m}_w$ was produced by draining a small fraction of flow through a bypass valve. A small perturbation should be applied since the collector dynamics is nonlinear with respect to the mass flowrate as shown by Eq. (2). This produces a consistency with the linearly perturbed model $G(s)$. Negative step changes around 15 – 20 percent from $\bar{m}_w$ were used in the present experiments.

2 Signal Processing. The pretreatment of I/O signals is required since the step signal is a power signal not directly Fourier transformable. Additionally, the measured output signal is $z(t)$ which consists of the noise $n(t)$ and the desired collector response $\tilde{T}_e(t)$ (Fig. 7). Filtering of the noise $n(t)$ from the measured signal $z(t)$ is thus necessary. A digital low-pass RC filter with a cutoff frequency of 0.025 Hz was used in the present study. The filtered output signal of $z(t)$, i.e., $\tilde{T}_e(t)$, is thus a summation of the responses of the disturbance model $v(t)$ and the plant model $y(t)$. That is,

$$\tilde{T}_e(t) = y(t) + v(t) \tag{43}$$

In identifying the disturbance model $W(s)$, we let $\tilde{m}_w(t) = 0$ and thus $y(t) = 0$. The negative step change of $\tilde{I}(t) = -\bar{I}u(t)$ then induces a response of $v(t) = \tilde{T}_e(t)$ which is a

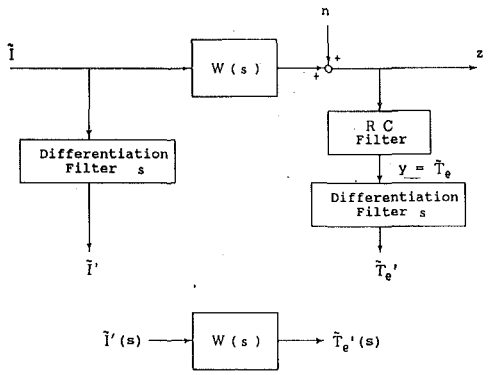

Fig. 8 Schematic diagram of the signal flow in identifying the disturbance model *W(s)*

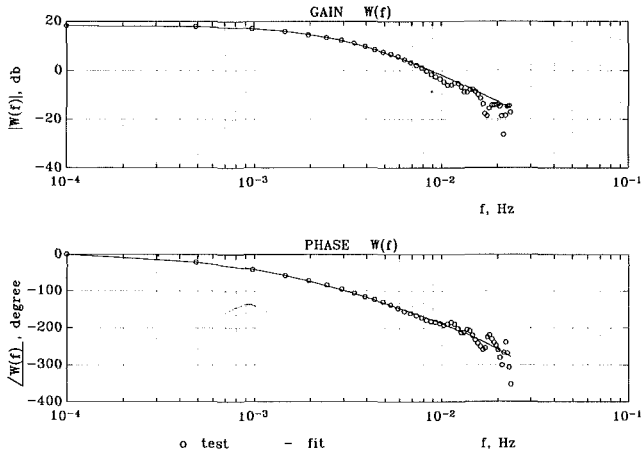

Fig. 9 Bode plot of $W(\omega)$ at $\bar{m}_w = 0.05151$ kg/s

low-pass filtered signal of $z(t)$. The frequency response of the model $W(s)$ is to be determined which defined as

$$W(\omega) \equiv \frac{\tilde{T}_e(\omega)}{\tilde{I}(\omega)}, \tag{44}$$

the output signal $\tilde{T}_e(t)$ and the step input signal $\tilde{I}(t)$ are first differentiated with respect to time to yield energy signals $\tilde{T}'_e(t)$ and $\tilde{I}'_T(t)$ which are directly Fourier transformable. And then, by Fourier transforms of the differentiated signals and noting that

$$\tilde{I}'_T(t) = -\bar{I}du(t)/dt = -\bar{I}\delta(t), \tag{45}$$

obtained here is

$$\tilde{T}'_e(\omega) = F[\tilde{T}'_e(t)] = j\omega\tilde{T}_e(\omega);$$
$$\tilde{I}'_T(\omega) = F[-\bar{I}\delta(t)] = -\bar{I}. \tag{46}$$

Noting that

$$\frac{\tilde{T}'_e(\omega)}{\tilde{I}'_T(\omega)} = \frac{j\omega\tilde{T}_e(\omega)}{j\omega\tilde{I}(\omega)} = \frac{\tilde{T}_e(\omega)}{\tilde{I}(\omega)} = W(\omega). \tag{47}$$

That is, the frequency response of the disturbance model $W(\omega)$ can be written in terms of the ratio of the frequency responses for the differentiated signals, $\tilde{T}'_e(\omega)$ and $\tilde{I}'_T(\omega)$ (Fig. 8). The identification using this input signal can assure accurate results since the differentiated input signal $\tilde{I}'_T(\omega)$ is persistently exciting as has been shown by Eq. (45). The use of step input signal in the system identification as being feasible is also verified by this (also refer to [9]). This concept was also applied in the identification of $G(s)$.

Combining Eq. (47) with (46), we obtain

$$W(\omega) = -\frac{\tilde{T}'_e(\omega)}{\bar{I}} = -\frac{j\omega\tilde{T}_e(\omega)}{\bar{I}}. \tag{48}$$

The frequency response of the disturbance model $W(\omega)$ can be evaluated by Eq. (48) since the differentiated output signal $\tilde{T}'_e(t)$ is an energy signal and can be easily computed via FFT. The circles shown in Fig. 9 are the Bode plot of the measured $W(\omega)$ at $\bar{m}_w = 0.05151$ kg/s. The phase plot of $W(\omega)$ is seen here to not oscillate around -180 deg at a frequency of < 0.01 Hz as shown in Fig. 3. It, however, tends to decrease and slightly oscillate at $f > 0.01$ Hz. This may result from the effects of time lag and unmodelled dynamics due to the use of the 2-node concept, the ignorance of wind speed effect and the assumptions of constant physical properties and uniform flow distribution in the collector etc. The oscillation may also result from the measurement noises.

Similarly, in identifying the plant model $G(s)$, we could let $\tilde{I}(t) = 0$ (i.e., run the test during steady irradiation) and hence $v(t) = 0$. The negative step change of $\tilde{m}_w(t) = -\Delta m_w u(t)$ thus induces a time response of $y(t) = \tilde{T}_e(t)$ which is a low-pass filtered signal of $z(t)$, where Δm_w is the magnitude of the step change of m_w. In fact, a perfect steady irradiation can hardly be obtained in an outdoor test. A signal pretreatment by subtracting the component induced by the disturbance model $W(s)$ is thus necessary. That is, the frequency response $Y(\omega)$ driven directly by the disturbance model $G(s)$ can be obtained by using the determined $W(\omega)$ and the following relation

$$Y(\omega) = \tilde{T}_e(\omega) - \tilde{I}(\omega)W(\omega) \tag{49}$$

Since the negative step input of mass flowrate is applied, $\tilde{m}_w = -\Delta m_w u(t)$, the frequency response of the plant model $G(\omega)$ can be obtained by using the similar differentiating filter and the following relation

$$G(\omega) = -\frac{\tilde{Y}'(\omega)}{\Delta m_w} = -\frac{j\omega Y(\omega)}{\Delta m_w}, \tag{50}$$

where $\tilde{Y}'(\omega)$ is the Fourier transform of $y'(t)$ where $y'(t)$ is the time differentiation of the time response $y(t)$ of the disturbance model $G(s)$. The frequency response $G(\omega)$ can be easily determined from Eq. (50) via FFT. The circles shown in Fig. 10 are the Bode plot of the measured $G(\omega)$ at $\bar{m}_w = 0.0543$ kg/s. The phase plot of $G(\omega)$ is seen here to not oscillate around -90 deg at a frequency of < 0.01 Hz as shown in Fig. 4. It, however, tends to decrease and oscillate at $f > 0.01$ Hz. This is also due to the effects of unmodelled dynamics and measurement noises.

The step inputs for $\tilde{I}$ and $\tilde{m}_w$ used in the present experiments have a rise time in the order of several seconds which are quite short as compared to the dynamic responses of the solar collector (approximately several minutes). The input signals are then pretty close to an ideal step function and

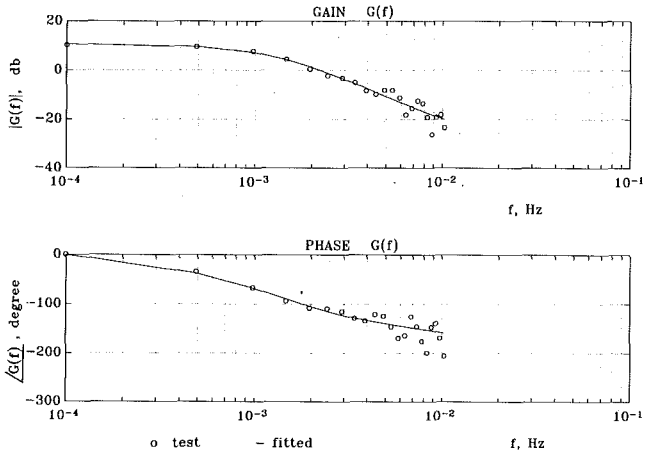

Fig. 10 Bode plot of $G(\omega)$ at $\overline{m}_w$ = 0.0543 kg/s

Table 2 Parameter estimation of the disturbance model $W(s)$

$\overline{I}$, W/m^2	$\overline{m}_w$, kg/s	k_I, °Cm²/kW	p_{I1}, s^{-1}	p_{I2}, s^{-1}	τ_{dI}, s
1044	0.01515	22.30	.007830	.007831	23.96
931	0.01924	19.71	.009572	.009579	20.19
1107	0.02732	14.18	.010527	.017301	18.69
995	0.04313	10.14	.012560	.033207	12.90
755	0.04531	8.75	.011677	.035003	14.85
843	0.05151	8.05	.012735	.035201	13.25
1016	0.05606	7.67	.012439	.044850	16.02

Table 3 Parameter estimation of the plant model $G(s)$

$\overline{I}$, W/m^2	$\overline{m}_w$, kg/s	z_w, s^{-1}	k_w, °Cs²/kg	p_{w1}, s^{-1}	p_{w2}, s^{-1}	τ_{dw}, s
749	0.0135	.0540	17.45	.009457	.009458	13.67
516	0.0276	.0425	4.816	.010760	.010660	13.58
719	0.0310	.0483	6.099	.012110	.011900	10.99
628	0.0382	.0609	3.761	.014510	.013950	11.06
961	0.0543	.0518	3.395	.008810	.008782	12.40

the frequency response results obtained in the present study will be accurate enough at a frequency of < 0.02 Hz.

3.3 Frequency-Domain Model Fitting. Since the dynamic model of flat-plate collector would have no unstable poles, the frequency responses measured above can then be used to fit the linear model, equations (36) and (37), in frequency domain to determine the system parameters τ_{dI}, k_I, p_{I1}, p_{I2}, τ_{dw}, k_w, p_{w1}, p_{w2}, z_w etc.

The frequency-domain model fitting was used in the present study by using a computer program developed by Seidel [10]. The parameters of $W(s)$ and $G(s)$ estimated at various operating conditions are respectively listed in Table 2 and 3. One of the frequency-domain model fitting results are presented in Figs. 9 and 10 which indeed shows a good fit.

3.4 Semi-empirical Correlation of System Parameters. The system parameters can be seen from Tables 2 and 3 to vary with steady-state operating conditions. However, the governing Eqs. (1) and (2) indicate that the system response T_e will vary linearly with the disturbance input I and nonlinearly with the controllable input m_w. Therefore, the linearized system parameters will essentially be a function of steady-state mass flowrate $\overline{m}_w$. The empirical correlations of the system parameters, in terms of a third-order polynomial of $\overline{m}_w$, can be derived as:

$$\theta = a_1 + a_2\overline{m}_w + a_3\overline{m}_w^2 + a_4\overline{m}_w^3 \qquad (51)$$

where θ represents the system parameters. Equation (51) was found to be able to be fitted very well. The coefficients a_1, a_2, a_3, a_4 for the disturbance model $W(s)$ and the plant model $G(s)$ are determined by a least-squares fit and shown in Table 4.

Table 4 Least-squares fit of the coefficients in Eq. (51)

	a_1	a_2	a_3	a_4
k_I	38.34	-1.36×10^3	2.13×10^4	-1.215×10^5
τ_{dI}	28.41	−216.1	-1.163×10^4	2.033×10^5
p_{I1}	1.785×10^{-3}	0.5587	−10.23	66.0
p_{I2}	-1.572×10^{-3}	0.4203	13.25	117.0
z_w	0.1690	−14.01	470.0	-4.644×10^3
k_w	47.34	-3.112×10^3	7.446×10^4	-5.910×10^5
p_{w1}	2.517×10^{-2}	−2.121	83.37	−920.5
p_{w2}	2.310×10^{-2}	−1.848	73.06	−810.1
τ_{dw}	6.894	936.3	-3.747×10^4	4.081×10^5

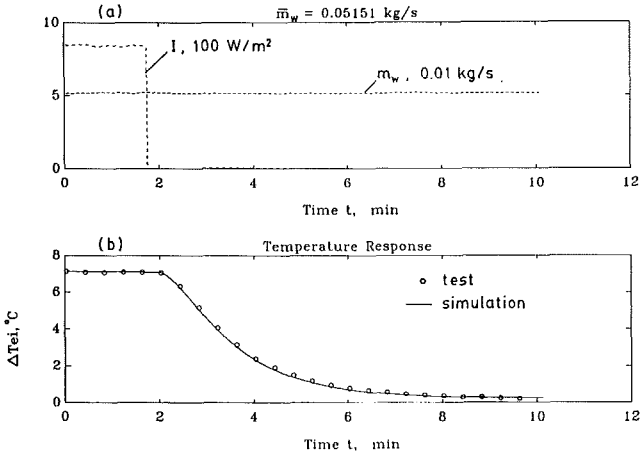

Fig. 11 Temperature response for step input $\overline{I}$ and simulation using $W(s)$ model with Eq. (51). (*a*) Input signals; (*b*) temperature response.

IV Discussion and Conclusion

The linear dynamic model, Eqs. (36) and (37), associated with the parameter correlations, Equation (51), will form a system dynamic model of flat-plate collectors with parameters varying with steady-state operating conditions. That is, the system dynamics model can trace the plant variation caused by a variation of operating conditions. The simulations using the present model, Eqs. (36) and (37), associated with the empirical correlations, Eq. (51), were shown to agree very well with the test results for the step response tests, as shown in Figs. 11 and 12.

The time response of the solar collector $T_e(t)$, which is subject to a random input signal $I(t)$, can also be predicted using this linear model. The results shown in Fig. 13 are a time response result of the collector. The agreement between the prediction and the measured data is indeed shown to be very good.

The methodology outlined in the present paper may be called *physical model-based approach* and is quite useful in deriving a dynamic model of systems having nonlinear

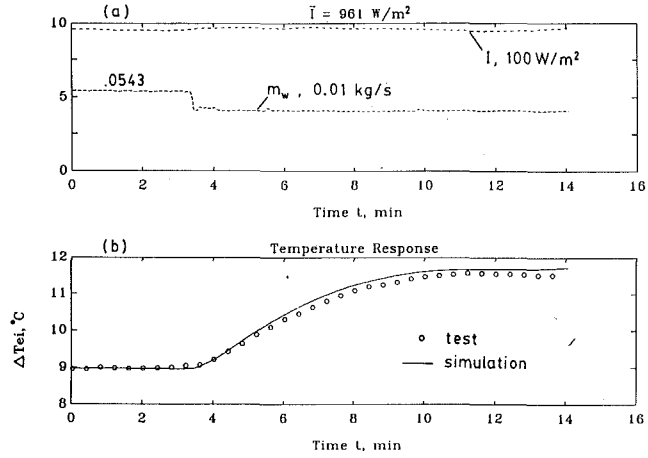

Fig. 12 Temperature response for step input $\bar{m}_w$ and simulation using $G(s)$ model with Eq. (51). (*a*) Input signals; (*b*) temperature response.

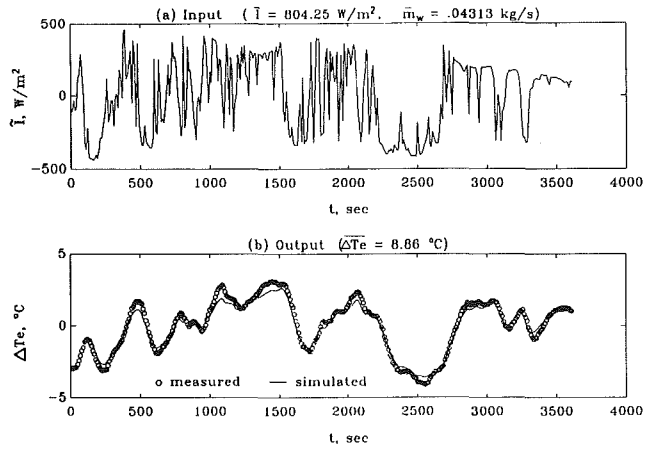

Fig. 13 Time-response of the collector subject to time-variant input

effects. The dynamic model derivation basically starts with a theoretical derivation of nonlinear governing equations by use of multiple nodes concept and physical principles. Linearization and Laplace transforms are employed to lead to a distributed system model. Model reduction or simplification in accordance with the physical phenomena which will be encountered during field applications is then carried out. A simple and comprehensible linear model will finally be obtained with system parameters such as poles, zeros, time delays etc. which are left to be determined experimentally. The identification of these system parameters can then be carried out by a step response test and a frequency response analysis associated with the model fitting technique in frequency domain. The dynamic tests and the parameters estimations are to be carried out at various operating conditions. An empirical correlation of the system parameters in terms of operating conditions can then be derived from these results.

Two nonlinear governing equations of the flat-plate collector were first derived based on the 2-node concept and energy conservation principle and a linearly perturbed dynamics model was then approximated here for leading to a distributed model. A model reduction was further employed to obtain a simple time-invariant linear model with poles, zeros, and time delay left to be determined experimentally. An outdoor test was then carried out to identify the system parameters by a frequency response analysis and model fitting in the frequency domain. To account for the variation of system dynamics behavior with the operating conditions (i.e., a nonlinear effect), the system parameters such as time delays, zeros and poles were identified at various operating conditions and the empirical correlations of these parameters in terms of the steady-state mass flowrate $\overline{m}_w$ were derived. Hence, the nonlinear effect due to the mass flowrate variation is taken into account and the identified system model can describe the system dynamics under various steady-state operating conditions.

Acknowledgment

The present study was supported by the National Science Council, Taiwan, the Republic of China, through Grant No. NSC78-0401-E002-18.

References

1 Close, D. J., "A Design Approach for Solar Processes," *Solar Energy*, Vol. 11, 1967, p. 112.

2 Klein, S., Duffie, J. A., and Beckman, W. A., "Transient Considerations of Flat-Plate Collectors," ASME Journal of Engineering for Power, Vol. 96, 1974, pp. 109–131.

3 de Ron, A. J., "Dynamic Modeling and Verification of a Flat-Plate Solar Collector," *Solar Energy*, Vol. 24, 1980, pp. 117–128.

4 Kawata, S., Kanoh, H., and Masubuchi, M., "A Correlation Between Steady-State and Dynamic Response of a Counterflow Heat Exchanger," ASME JOURNAL OF DYNAMIC SYSTEMS, MEASUREMENT, AND CONTROL, Vol. 111, 1989, pp. 115–118.

5 Cohen, W. C., and Johnson, E. F., "Distributed Parameter Process Dynamics," *Chem. Eng. Progress Symp. Series*, No. 36, Vol. 57, 1956, pp. 86–99.

6 Willams, T. J., and Morris, H. J., "A Survey of the Literature on Heat Exchanger Dynamics and Control," *Chem. Eng. Progress Symp. Series*, No. 36, Vol. 57, 1956, pp. 20–32.

7 Huang, B. J., and Hsieh, S. W., "An Automation of Collector Testing and Modification of ANSI/ASHRAE 93-1986 Standard." ASME *Journal of Solar Energy Engineering*, Vol. 116, 1990, pp. 257–267.

8 Huang, B. J., "A Precise Measurement of Temperature Difference Using Thermopiles," *Experimental Thermal and Fluid Science*, Vol. 3, 1990, pp. 265–271.

9 Rade, H., "Step Response and Frequency Response Methods," *Automatica*, Vol. 16, 1980, pp. 519–526.

10 Seidel, R. C., "Transfer-Function-Parameter Estimation from Frequency Response Data—A Fortran Program," NASA TM X-3286, 1975.